

Effects of Water/Alcohol Soluble Cationic Polythiophenes as Cathode Interlayers for Eco-Friendly Solar Cells

Debora Quadretti, Martina Marinelli, Elisabetta Salatelli, Filippo Pierini, Alberto Zanelli, and Massimiliano Lanzi*

Three new ionic polythiophene derivatives, soluble in polar solvents, are synthesized with good yields using simple, low-cost, and straightforward procedures. They are investigated as interfacial cationic conjugated polyelectrolyte (CPE) layers for halogen-free bulk heterojunction polymeric solar cells, based on a water-soluble electron-donor polymer (poly[3-(6-diethanolaminoethyl)thiophene]) and a water-soluble electron-acceptor fullerene derivative (malonodiserinamide fullerene). The simple insertion of the CPE interlayer between the active layer and the aluminum cathode dramatically increases the power conversion efficiency of the final device up to nearly 5%, resulting from a decrease of the electrode work function, improved electron extraction, and optimization of the morphology of the layers. The obtained results demonstrate that the incorporation of CPE layer is a powerful and convenient methodology for the development of highly efficient and eco-friendly processable polymeric solar cells.

In the last decades, different types of devices with several architectures have been developed, obtaining the best results using bulk heterojunction (BHJ) solar cells.^[3] In this model, the photoactive layer—placed between an indium-tin oxide (ITO) anode and an aluminium cathode—is made of an electron-donor (ED, a π -conjugated polymer) and an electron-acceptor (EA, usually a fullerene derivative) material mixed in the same bulk. The main feature of a BHJ device is indeed the possibility to combine easy processability with high final efficiency, as the enhanced interface area between the two components promotes an efficient generation and transport of free-charge carriers.^[4]

To avoid oxidation phenomena and improve hole extraction and collection, the

photoactive layer is typically not placed in direct contact with the anode, but a hole transport layer (HTL) is commonly deposited between the ITO and the active layer.^[5] The most used HTL is made of poly(3,4-ethylenedioxythiophene):poly(styrenesulfonate) (PEDOT:PSS) due to its eco-friendly solution processability, high conductivity, stability, and high light transmittance.^[6]

Otherwise, in common BHJ solar cells, the photoactive layer is directly in contact with the cathode surface, with possible migration of metal atoms into the active layer during deposition and subsequent decrease of the open-circuit voltage (V_{oc}).^[7] Therefore, to avoid these drawbacks and increase the power conversion efficiency (PCE) and V_{oc} of BHJ devices, several polymeric electrolytes (i.e., polythiophene^[8] and polyfluorene^[9] derivatives) with different pendant cationic moieties (i.e., trimethylammonium group) have been used as interlayers between the photoactive and cathode films to modify the interface.^[10,11] The presence of an ionic moiety on the conjugated polyelectrolyte—acting as an electron transporting layer (ETL)—seems to improve the final performance of the device by changing the interactions at the cathode interface due to the increase of polarity. In fact, the consequently modified dipole moment^[12]—which generates a capacitive double layer—allows an easier charge transport and collection.^[13,14] The reduction of the work function of the cathode^[15] results in a lower resistance at the interface, thus leading to a higher fill factor (FF), short-circuit current density (J_{sc}), open-circuit voltage (V_{oc}), and, consequently, power conversion efficiency. Moreover, the recombination is reduced due to better charge carriers' mobility.^[16]

1. Introduction

In the burgeoning field of photovoltaic, conjugated polymer solar cells (PSCs) have drawn attention and have been widely studied for their features and advantages, such as structural versatility of the organic material, light weight, flexibility, and low cost.^[1] These devices can convert sunlight into electrical energy through a mechanism that provides light absorption, the generation of charged carriers, and their subsequent separation and transport with final collection to the respective electrodes.^[2]

D. Quadretti, M. Marinelli, E. Salatelli, M. Lanzi
 Department of Industrial Chemistry "Toso Montanari"
 University of Bologna
 Viale Risorgimento 4, Bologna (BO) 40136, Italy
 E-mail: massimiliano.lanzi@unibo.it

F. Pierini
 Department of Biosystem and Soft Matter
 Institute of Fundamental Technological Research Polish Academy of Science
 ul. Pawinskiego 5B, Warsaw 02-106, Poland

A. Zanelli
 National Research Council (CNR) – Institute for Organic Synthesis and Photoreactivity (ISOF)
 Via Piero Gobetti 101, Bologna (BO) 40129, Italy

 The ORCID identification number(s) for the author(s) of this article can be found under <https://doi.org/10.1002/macp.202200422>

DOI: 10.1002/macp.202200422

Another interesting feature is the solubility of polymer electrolytes in environmental-friendly polar solvents such as alcohols—usually methanol, ethanol, isopropanol—and water. The possibility to process both the photoactive layer and the interlayer from more green solvents means that the sustainability of the final device considerably increases. For this reason, in recent years, the attention has been widely focused on water/alcohol soluble conjugated polymers (WSCPs)^[17,18] and their application in several fields such as biosensors,^[19] chemical sensors,^[20] polymeric light-emitting diodes,^[21] and PSCs.^[22]

In view of the foregoing, we here report the synthesis and study of three different thiophene-based cationic interlayers soluble in green polar solvents: poly[3-(6-tributylphosphoniumhexyl)thiophene]bromide (PT6buP⁺Br⁻), poly[3-(6-tributylphosphoniumhexyloxy)thiophene]bromide (PTO6buP⁺Br⁻), and poly(6-tributylphosphoniumhexyl-1-oxymethyl-EDOT)bromide (P(EDOT-MeO6buP⁺Br⁻)). Besides, we compare the photoconversion efficiencies of completely eco-friendly BHJ devices, obtained by testing the prepared materials as ETL, in the presence of a nonionic photoactive layer which is also processable from alcohols and water (blend of poly[3-(6-diethanolaminoethyl)thiophene] (PT6N(EtOH)₂) with malonodiserinamide-derivatized fullerene (C₆₀-Ser). PT6N(EtOH)₂ was chosen as the photoactive polymer since it has been recently reported that the presence of ionic groups in the photoactive blend may induce disorder at the macromolecular level in the solid state or act as traps for charges, thus leading to unsatisfactory PCE values.^[23]

The structural and photophysical properties of the synthesized precursor and alcohol-soluble polymers were investigated using nuclear magnetic resonance (NMR), infrared (FT-IR), and ultraviolet–visible (UV–vis) spectroscopy, in addition to thermogravimetric analysis (TGA), differential scanning calorimetry (DSC), cyclic voltammetry (CV), X-ray diffraction (XRD), atomic force microscopy (AFM), and external quantum efficiency (EQE). The final materials were tested in organic solar devices prepared with halogen-free solvents, obtaining an increase of photoconversion efficiency value up to 55% when PT6N(EtOH)₂:C₆₀-Ser and PTO6buP⁺Br⁻ were used as a photoactive layer and conjugated polyelectrolyte (CPE), respectively, in comparison with the same cell devoid of any interlayer.

2. Experimental Section

2.1. Materials

Tributylphosphine (97%), 1,6-hexandiol (99%), tetrahydrofuran (THF, >99.9%), toluene (C₇H₈, >99.9%), diethyl ether (Et₂O, >99.5%), ethyl acetate (EtOAc, >99.5%), hydroxymethyl EDOT, 3-methoxythiophene (98%), and chloroform (CHCl₃, 99.0–99.4%) were purchased from Sigma-Aldrich Chemical Co. (USA). Petroleum ether (Etp, >90%) was purchased from Sigma-Aldrich (Israel). *N,N*-Dimethylformamide (≥99.8%) and sodium hydroxide (NaOH, ≥98%), were purchased from Sigma-Aldrich (Germany). Hexane (≥99%) and dichloromethane (≥99.9%) were purchased from Sigma-Aldrich (France). Nitromethane (CH₃NO₂, ≥98.5%), tetrabutylammonium bromide (TBAB, ≥99%), hydrobromic acid (HBr, 48%), hydrochloric acid (HCl, ≥37%), and ferric chloride (FeCl₃, ≥98%) were purchased

from Fluka (Switzerland). Diethanolamine (DEA, 99%) was purchased from Aldrich. 1,6-Dibromohexane (B6B, >97%) was purchased from TCI (Tokyo). *p*-Toluenesulfonic acid monohydrate was purchased from Carlo Erba (Italy). Sodium sulfate (Na₂SO₄, anhydrous) and sodium bicarbonate (NaHCO₃) were purchased from Riedel-de Haën (Poland). Methanol (MeOH, >99.8%) was purchased from Honeywell (Germany). Deuterated chloroform (CDCl₃) and deuterated methanol (CD₃OD) were supplied by Sigma-Aldrich (Italy). 6-bromo-1-hexanol (B6OH) was synthesized as reported in the work of Chang et al.^[24] Regioregular poly[3-(6-bromohexyl)thiophene] (rrPT6Br) was synthesized through Grignard Metathesis Polymerization (GRIM).^[25] 3-(6-Bromohexyl)thiophene (T6Br) synthesis and subsequent oxidative polymerization with FeCl₃ to give non-regioregular poly[3-(6-bromohexyl)thiophene] (PT6Br) were performed according to the previously reported methods.^[26] Poly[3-(6-diethanolaminoethyl)thiophene] (PT6N(EtOH)₂) was synthesized according to the procedure reported in literature (95% HT, Mn = 9.9 kDa, PDI = 1.3).^[27] Synthesis of 6-bromohexyl-1-oxymethyl-EDOT (EDOT-MeO6Br) and purification of P(EDOT-MeO6Br) were carried out accordingly to the procedure reported in literature.^[28,29] Malonodiserinamide fullerene (C₆₀-Ser) was prepared according to previously reported literature methods.^[30] To remove the stabilizer, diethyl ether and THF were freshly distilled before the use. The procedures involving air/moisture-sensitive reagents were performed under argon atmosphere.

2.2. Synthesis of Cationic Polythiophene Interlayers

2.2.1. General Procedure for Oxidative Polymerization with FeCl₃

In a three-neck flask, the monomer was dissolved in anhydrous chloroform under inert atmosphere, and a solution of FeCl₃ in CH₃NO₂ was added dropwise to the system (10 min) and the mixture was allowed to react under a flux of argon for 40 min at room temperature. Afterward, THF was added, and the system stirred for further 50 min.

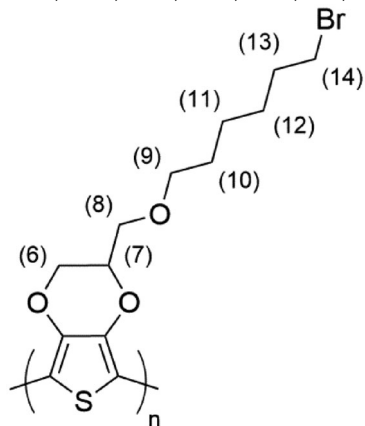
The mixture was poured into 300 mL of MeOH/HCl (5% v/v), and the precipitated product was recovered by filtration on a PTFE membrane (0.45 μm pore size). The obtained solid was then dissolved in CHCl₃, washed with HCl 2% up to exhaustive extraction of the iron (III) ion (negative NH₄SCN test), and several times with water up to neutrality. The organic phase was dried over Na₂SO₄, filtered, and the solvent was removed under reduced pressure.

In the case of P(EDOT-MeO6Br) the darkish solid was recovered in CHCl₃ (5 mg mL⁻¹), added to a solution of ammonium hydroxide (1:1), and heated until reflux conditions for 2 h. The organic phase was washed several times with distilled water until neutrality, dried with Na₂SO₄, filtered, and concentrated under reduced pressure.

Poly[3-(6-bromohexyl)thiophene] (PT6Br): Starting from 450 mg (1.82 mmol) of 3-(6-bromohexyl)-thiophene (T6Br) in 25.0 mL of anhydrous CHCl₃, the addition of 1.18 g (7.28 mmol) of FeCl₃ in 7.50 mL of CH₃NO₂ gave 250 mg (1.02 mmol) of PT6Br as a reddish solid (yield 56%, 85% HT, Mn = 9.8 kDa, PDI = 1.9). ¹H-NMR (CDCl₃, ppm): δ 6.98 (s, 1H, Th H4), 3.43 (bt, 2H, CH₂Br), 2.82, 2.58 (bt, 2H, ThCH₂), 1.96–1.80 (m,

2H, $\text{CH}_2\text{CH}_2\text{Br}$), 1.80-1.64 (m, 2H, ThCH_2CH_2), 1.60-1.36 (m, 4H, $(\text{CH}_2)_2$). $^{13}\text{C-NMR}$ (CDCl_3 , ppm): δ 143.71, 143.01, 141.03, 140.28 (Th C3), 136.94, 135.88, 134.61, 134.77 (Th C5), 131.32, 130.85, 130.23, 129.85 (Th C2), 129.04, 128.65, 128.32, 127.63 (Th C4), 34.55 (CH_2Br), 33.81 ($\text{CH}_2\text{CH}_2\text{Br}$), 30.94 (ThCH_2), 29.96, 29.15, 28.53 (aliphatic CH_2). FT-IR (Ge, cm^{-1}): 3055, 2929, 2854, 1509, 1457, 1259, 1090, 827, 727, 645, 562.

Poly[3-(6-bromohexyloxy)thiophene] (PTO6Br): Starting from 300 mg (1.14 mmol) of 3-(6-bromohexyl-1-oxy)thiophene (TO6Br) in 25.0 mL of anhydrous CHCl_3 , the addition of 755 mg (4.65 mmol) of FeCl_3 in 4.73 mL of CH_3NO_2 gave 133 mg (0.509 mmol) of a reddish solid (yield 45%, 68% HT, Mn = 2.3 kDa, PDI = 1.8). $^1\text{H-NMR}$ (CDCl_3 , ppm): δ 7.03-6.70 (b, 1H, Th H4), 4.16, 3.93 (2bm, 2H, ThOCH_2), 3.42 (bm, 2H, CH_2Br), 2.12-1.74 (bm, 4H, $\text{ThOCH}_2\text{CH}_2$ and $\text{CH}_2\text{CH}_2\text{Br}$), 1.73-1.27 (bm, 4H, aliphatic CH_2). $^{13}\text{C-NMR}$ (CDCl_3 , ppm): δ 154.82 (Th C3), 136.32 (Th C5), 107.99 (Th C4), 106.72 (Th C2), 68.00, 67.78 (ThOCH_2), 32.67 (CH_2Br), 29.85 ($\text{ThOCH}_2\text{CH}_2$), 30.04, 28.14, 24.16, 23.04 (aliphatic CH_2). FT-IR (Ge, cm^{-1}): 3079, 2937, 2860, 1520, 1456, 1222, 1191, 1071, 829, 734, 645, 562.



Poly(6-bromohexyl-1-oxymethyl-EDOT) [P(EDOT-MeO6Br)]: Starting from 262 mg (0.782 mmol) of 6-bromohexyl-1-oxymethyl-EDOT (EDOT-MeO6Br) in 13.0 mL of anhydrous CHCl_3 , the addition of 517 mg (3.13 mmol) of FeCl_3 in 2.36 mL of CH_3NO_2 gave 80.0 mg (0.240 mmol) of a dark purple solid (yield 31%, 81% HT, Mn = 4.3 kDa, PDI = 1.7). $^1\text{H-NMR}$ (CDCl_3 , ppm): δ 4.76-3.93 (bm, 3H, H7 and H6), 3.92-3.62 (b, 2H, H8), 3.49 (bs, 2H, H9), 3.41 (bs, 2H, H14), 1.85 (bs, 2H, H13), 1.59 (bs, 2H, H10), 1.50-1.24 (bm, 4H, H11 and H12). $^{13}\text{C-NMR}$ (CDCl_3 , ppm): 143.87 (Th C3+C4), 121.70 (Th C2+C5), 82.70 (C7), 81.89 (C8), 77.57 (C9), 72.18 (C6), 34.22 (C14), 32.99, 29.74, 28.28, 25.57 (aliphatic CH_2). FT-IR (Ge, cm^{-1}): 2935, 2862, 1460, 1438, 1305, 1240, 1225, 1117, 1057, 913, 841, 751, 643, 561.

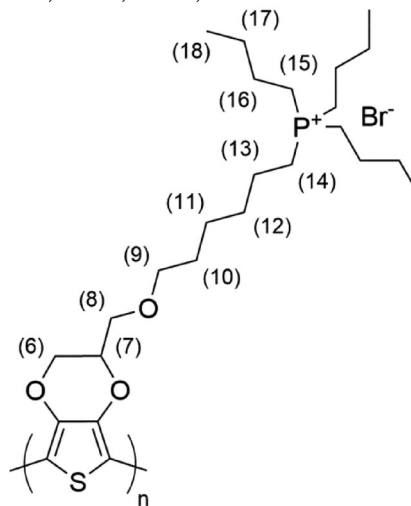
2.2.2. General Procedure for the Postfunctionalization of Brominated Polymers with Tributylphosphine

The brominated polymeric precursor was dissolved in toluene in a three-neck flask and then tributylphosphine was added to the system under stirring and in an inert atmosphere. After reacting at 90 °C for 24 h, the supernatant was removed, and the film formed on the flask surface was recovered with methanol. The solvent was evaporated under reduced pressure, and the product

was washed several times with diethyl ether and dried under vacuum to give the final cationic polymer.

Poly[3-(6-tributylphosphoniumhexyl)thiophene]bromide (PT6buP⁺Br⁻): Starting from 360 mg (1.47 mmol) of PT6Br in 20.0 mL of toluene, the addition of 3.60 mL (14.6 mmol) of tributylphosphine gave 636 mg (1.42 mmol) of PT6buP⁺Br⁻ as a dark red solid (yield 97%). $^1\text{H-NMR}$ (CD_3OD , ppm): δ 7.14 (s, 1H, Th H4), 2.90, 2.64 (bs, 2H, ThCH_2), 2.25 (bs, 8H, $\text{CH}_2\text{P}^+\text{CH}_2$), 1.85-1.71 (bm, 2H, ThCH_2CH_2), 1.70-1.43 (bm, 18H, $(\text{CH}_2)_n$) 0.98 (bt, 9H, CH_3). $^{13}\text{C-NMR}$ (CD_3OD , ppm): δ 141.62 (Th C3), 134.92 (Th C5), 131.67 (Th C2), 130.28 (Th C4), 31.49, 30.18, 29.74, 25.10, 24.94, 24.50, 22.49 (aliphatic CH_2), 19.54 (CH_2P^+), 19.08 (P^+CH_2), 13.88 (CH_3). $^{31}\text{P-NMR}$ (CD_3OD , ppm): δ 33.86. FT-IR (Ge, cm^{-1}): 3053, 2957, 2929, 2870, 1513, 1463, 1410, 1378, 1232, 1099, 833, 723. Elemental analysis: calcd for $[(\text{C}_{22}\text{H}_{40}\text{BrPS})]_n$ C 59.05, H 9.01, S 7.17, P 6.92, Br 17.85. Found: C 59.09, H 8.89, S 7.80, P 6.88, Br 17.94.

Poly[3-(6-tributylphosphoniumhexyloxy)thiophene]bromide (PTO6buP⁺Br⁻): Starting from 120 mg (0.458 mmol) of PTO6Br in 8.00 mL of toluene, the addition of 1.14 mL of tributylphosphine gave 198 mg (0.428 mmol) of PTO6buP⁺Br⁻ as a dark-red solid (yield 93%). $^1\text{H-NMR}$ (CD_3OD , ppm): δ 7.08 (b, 1H, Th H4), 4.24-4.05 (2bm, 2H, ThOCH_2), 2.31-1.99 (bm, 8H, CH_2P^+), 1.98-1.82 (bm, 2H, $\text{ThOCH}_2\text{CH}_2$), 1.70-1.29 (bm, 18H, $(\text{CH}_2)_2\text{CH}_2\text{P}^+$), 1.01-0.82 (bm, 9H, CH_3). $^{13}\text{C-NMR}$ (CD_3OD , ppm): δ 140.76 (Th C3), 133.45 (Th C5), 129.82 (Th C2), 127.96 (Th C4), 66.90 (ThOCH_2), 28.16, 27.52, 25.27, 25.12, 24.91, 24.62 (aliphatic CH_2), 19.49 (CH_2P^+), 18.89 ($^+\text{PCH}_2$), 13.90 (CH_3). $^{31}\text{P-NMR}$ (400 MHz, ppm): δ 33.88. FT-IR (Ge, cm^{-1}): 3028, 2957, 2932, 2871, 1536, 1463, 1407, 1379, 1229, 1194, 1078, 831, 727. Elemental analysis: calcd for $[(\text{C}_{22}\text{H}_{40}\text{BrOPS})]_n$ C 57.01, H 8.70, O 3.45, S 6.92, P 6.68, Br 17.24. Found: C 57.07, H 8.67, O 3.43, S 6.89, P 6.71, Br 17.23.



Poly(6-tributylphosphoniumhexyl-1-oxymethyl-EDOT)bromide [P(EDOT-MeO6buP⁺Br⁻): Starting from 100 mg (0.300 mmol) of P(EDOT-MeO6Br) in 11.0 mL of toluene, the addition of 750 μL of tributylphosphine gave 142 mg (0.266 mmol) of a red cherry solid (yield 88%). $^1\text{H-NMR}$ (CD_3OD , ppm): δ 4.36-4.02 (b, 2H, H7 and H6), 3.95-3.65 (bm, 2H, H8), 3.64-3.36 (b, 2H, H9), 2.24 (bs, 8H, H14 and H15), 1.90-1.72 (bm, 2H, H10), 1.70-1.33 (bm, 18H, aliphatic CH_2), 0.98 (m, 9H, H18). $^{13}\text{C-NMR}$ (CD_3OD ,

ppm): 137.82 (Th C3+C4), 115.57 (Th C2+C5), 72.80 (C7), 70.29 (C8), 64.98 (C9), 60.76 (C6), 31.63, 30.51, 28.10, 27.45, 25.07, 22.46 (aliphatic CH₂), 19.48 (C14), 19.04 (C15), 13.90 (C18). ³¹P-NMR (CD₃OD, ppm): δ 33.90. FT-IR (Ge, cm⁻¹): 2957, 2932, 2870, 1462, 1439, 1379, 1311, 1231, 1226, 1115, 1052, 916, 835, 749. Elemental analysis: calcd for [(C₂₅H₄₄BrO₃PS)_n] C 56.07, H 8.28, O 8.96, S 5.99, P 5.78, Br 14.92. Found: C 56.12, H 8.22, O 8.95, S 5.94, P 5.74, Br 15.03.

2.3. Measurements

NMR spectra (¹H-NMR, ¹³C-NMR, and ³¹P-NMR) were recorded on a Varian Mercury Plus 400 spectrometer using TMS as a reference. IR spectra were taken on KBr or Ge disks using a Perkin Elmer Spectrum One spectrophotometer. UV-vis spectra were recorded on a Perkin Elmer Lambda 19 spectrophotometer using 10⁻⁵ M polymer solutions in spectroquality solvents in Suprasil quartz cuvettes (1 × 1 cm) or films on quartz slides. Elemental analyses were performed by Redox Laboratories, Monza, Italy.

The molecular weight of precursor polymers was determined by gel permeation chromatography (GPC) using THF solutions on a Lab Flow 2000 apparatus equipped with a Rheodyne 7725i injector, a Phenomenex MXL 5 μm mixed bed column, and a K-2301 KNAUER detector. The calibration curve was recorded using monodisperse polystyrene standards. Thermogravimetric analyses were recorded on NETZSCH TG 209 F1 Libra operating in air flux, which was used to determine the sample decomposition temperatures by heating from 30 to 600 °C with a ramp of 10 °C min⁻¹.

A TA Instruments Q2000 differential scanning calorimeter was used for the thermal analysis by varying the temperature from -20 to 200 °C with a heating and cooling ramp of 10 °C min⁻¹ in a nitrogen atmosphere.

Cyclic voltammeteries were performed with an AMEL 5000 electrochemical system at 0.1 V s⁻¹ in acetonitrile/toluene (25:75) v/v solutions with (C₄H₉)₄NClO₄ (0.1 mol L⁻¹) as supporting electrolyte in a three-compartment glass cell at room temperature under Ar pressure. Polymer films were deposited on Pt disk electrode (diameter 1 mm) by drop casting from methanol solutions. Auxiliary electrode was Pt spiral and potential reference was aqueous Saturated Calomel Electrode (SCE) whose absolute potential was assumed -4.24 V.^[31]

X-ray diffraction (XRD) data were recorded at room temperature by using a Cu Kα (λ = 1.5406 Å) radiation source (Philips PW 1050) and a Bragg-Brentano diffractometer (Philips PW 1710) equipped with a graphite monochromator in the diffracted beam. The 2θ range between 2.0° and 90.0° was scanned by 881 steps of 0.1° with a counting time of 15 s for each step. The XRD characterization was carried out on polymer films on glass slides deposited by doctor blading (100 nm average thickness) after an annealing procedure (heating at 120 °C for 30 min under vacuum).

The sample surface topography was evaluated with an atomic force microscope (AFM, Ntegra NT-MDT) equipped with a silicon cantilever (HA_NC, NT-MDT, tip radius of 10 nm, and spring constant of 12 N m⁻¹). Measurements were performed in a semi-contact mode with a resonance frequency of around 150 kHz; the scanning rate was 0.5 Hz, while the size of the scanned sample was 10 μm × 10 μm per image.

2.3.1. Solar Cells

Photovoltaic devices were prepared by the following procedure: the ITO glass substrate (2.0 × 2.0 cm, surface resistance 21 Ω sq⁻¹) was etched on one side using a 10% wt aqueous solution of HCl at 60 °C to obtain an area of 1.5 × 1.0 cm covered by indium tin oxide. The glass was then cleaned with distilled water and 2-propanol and dried with a nitrogen flow giving a final resistance of the ITO glass of 12 Ω sq⁻¹. PEDOT:PSS (2.8 wt% dispersion in water, viscosity 20 cps) was diluted 1:1 v/v with 2-propanol, sonicated for 15 min using an ultrasonic bath (Elmasonic S 30H), filtered on a Gooch G2, and the resulting solution (viscosity 12 cps) deposited over the previously treated ITO glass with the doctor blading technique using a Sheen Instrument Model S265674, leaving only a small (0.5 × 1.0 cm) area uncovered at the opposite side of the previously etched area.

The PEDOT:PSS film was heated in a Buchi GKR-50 glass oven at 120 °C for 90 min under vacuum (10⁻³ mmHg). A solution made by mixing 2.5 mg of PT6N(EtOH)₂ and 2.5 mg of C₆₀-Ser in 0.5 mL of methanol was sonicated and deposited by doctor blading on the slide in order to cover the PEDOT:PSS layer. Subsequently, the sample was annealed in the glass oven under vacuum (10⁻³ mmHg) at 120 °C for 30 min. A solution of 1.0 mg of cationic polymer (CPE) in 0.5 mL of ethanol was deposited on the photoactive layer by spray coating (Gohelper Mini Kit Airbrush, nozzle diameter 0.3 mm) and annealed at 120 °C for 15 min. Finally, a 50 nm-thick Al electrode was deposited over the polymeric layer through a shadow mask using an Edwards 6306A coating system operating at 10⁻⁶ mmHg. The active area of the cell was 1.0 × 1.0 cm². The current-voltage characteristics were measured in air using a Keithley 2401 source meter under the illumination of an Abet Technologies LS150 Xenon Arc Lamp Source AM 1.5 Solar Simulator (100 mW cm⁻²) calibrated with an ILT 1400-BL photometer. The structure of the final devices was: ITO (80 nm)/PEDOT:PSS (100 nm)/active layer (150 nm)/cationic interlayer (20 nm)/Al (50 nm). The solar cell spectral response (External Quantum Efficiency, EQE) was measured using a 7-SC Spec III Modularized Solar Cell Spectral Test System (SevenStar Optics, Beijing, PRC). Layer thicknesses were measured with an FTPAdvances FTPadv-2 Film Thickness Probe (Sentech GmbH, Germany) equipped with the FTPEXPERT software.

3. Results and Discussion

3.1. Synthesis

The ED material was synthesized through the postfunctionalization of regioregular poly[3-(6-bromohexyl)thiophene] (rrPT6Br) with diethanolamine (see Supporting Information), giving the corresponding poly[3-(6-diethanolaminohexyl)thiophene] (PT6N(EtOH)₂) as a neutral water/alcohol-soluble polymer.^[32] The choice of this photoactive material—instead of the most used poly(3-hexylthiophene)—has been made with the aim to prepare a completely eco-friendly photovoltaic device (photoactive blend and interlayers) avoiding the use of harmful solvents. For this purpose, the EA material C₆₀-Ser—a fullerene derivative soluble in polar solvents—was synthesized according to a

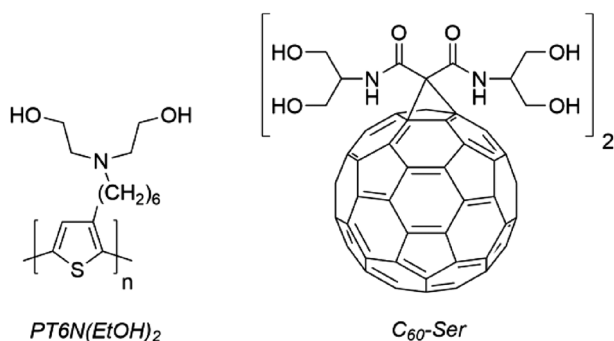


Figure 1. Chemical structure of poly[3-(6-diethanolaminoethyl)thiophene] (ED) and C₆₀-Ser (EA).

previous work.^[30] The structure of the synthesized electron-donor and electron-acceptor materials are reported in **Figure 1**.

The synthetic approach followed to prepare ionic materials was based on two main strategies: polymerization of monomers in the same conditions through oxidative reaction with FeCl₃ and subsequent postfunctionalization with the same substituent (tributylphosphine) as depicted in **Scheme 1**.

In detail, monomers 3-(6-bromohexyl)thiophene (T6Br), 3-(6-bromohexyl-1-oxy)thiophene (TO6Br), and 6-bromohexyl-1-oxymethyl-EDOT (EDOT-MeO6Br) were reacted with FeCl₃ in dry chloroform for 50 min under inert conditions.

The number average molecular weight (M_n) and the polydispersity index (Đ) were determined by GPC analysis of the soluble fraction of the synthesized precursor polymers (**Table 1**). The comparison between PT6Br and the other two polymers shows the obtainment of lower molecular weights for the latter, and this can be ascribed to the presence of alkoxy-groups grafted on the thiophene ring. In this case, the electron-donating effect of the oxygen stabilizes the radicals involved in the oxidative polymerization thus favoring the formation of shorter polymeric chains.^[33]

Finally, the postfunctionalization reaction of precursors (PT6Br, PTO6Br, and P(EDOT-MeO6Br)) with tributylphosphine of the bromoalkylic side chains was carried out at 90 °C for 24 h leading to the complete postfunctionalization of side-chain substituents.^[34] The reaction of precursor polymers with tributylphosphine has been chosen since phosphine usually leads to the complete postfunctionalization of bromine in the side chains, giving an optimal solubility of the resulting materials in polar solvents.^[35] Then the prepared cationic polymers have been employed as interlayers for polymeric solar cells since several recent studies report the use of conjugated polyelectrolytes (CPEs)—which combine the presence of a delocalized π-π* conjugated backbone with pendant ionic groups—as promising cathode interface modifiers.^[36]

3.2. NMR and FT-IR Spectroscopy

All the synthesized polymers were characterized by NMR spectrometry (¹H-NMR, ¹³C-NMR, and ³¹P-NMR for materials with phosphonium side group) to confirm their chemical structure (see Figure S1–S14, Supporting Information).

The analysis of ¹H-NMR spectra (**Figure 2**), recorded in CD₃OD, shows the total absence of methylenic protons in α position to -Br group, evidencing the successful postfunctionalization of precursors with tributylphosphine. In particular, the presence of a broad multiplet at 2.36–2.15 ppm, 2.31–1.99 ppm, and 2.24 ppm, for PT6buP⁺Br⁻, PTO6buP⁺Br⁻, and P(EDOT-MeO6buP⁺Br⁻), respectively, can be ascribed to the eight methylenic protons near to the phosphine moiety, thus confirming the substitution of bromide group.

The occurrence of the postfunctionalization of precursors was further verified by both ¹³C-NMR and ³¹P-NMR spectroscopy. Moreover, the ³¹P-NMR spectra evidence the absence of unreacted tributylphosphine and the complete substitution with phosphonium as previously verified by ¹H-NMR.

FT-IR spectroscopy further confirms the chemical structure of all synthesized materials. The FT-IR bands of interlayers (PT6buP⁺Br⁻, PTO6buP⁺Br⁻, and P(EDOT-MeO6buP⁺Br⁻)) and photoactive material (PT6N(EtOH)₂) with their assignments are shown in Tables S1–S4 of the Supporting Information.

In detail, the presence of bands ascribable to phosphonium group (≈1379 cm⁻¹) in IR spectra of PT6buP⁺Br⁻, PTO6buP⁺Br⁻, and P(EDOT-MeO6buP⁺Br⁻) (**Figure 3**) and the absence of peaks ascribable to -Br terminal group (≈640 and 560 cm⁻¹) confirm the successful reaction of postfunctionalization with the tributylphosphine group.

The broad band at ≈3400 cm⁻¹ (O–H stretching) is due to the high hygroscopicity of synthesized polymers thus confirming their high affinity for polar solvent (water).

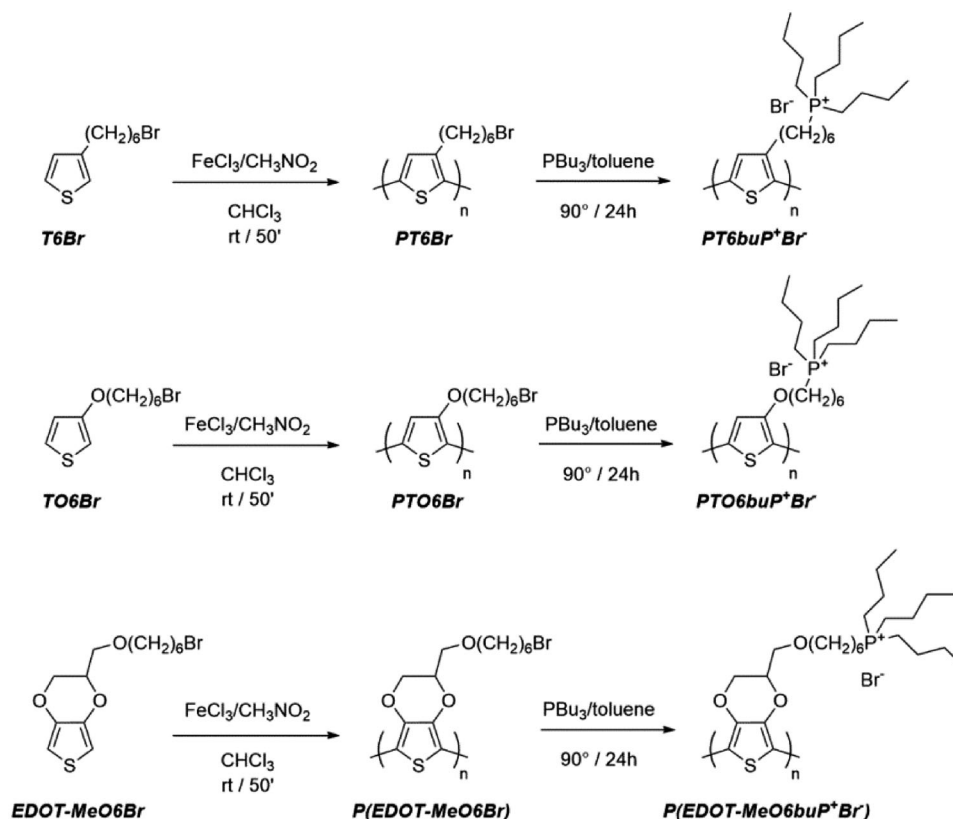
3.3. Thermal Properties

The thermal stability of interlayers and photoactive polymer has been evaluated by TGA analysis under oxidizing atmosphere (air), at a heating scan rate of 10 °C min⁻¹ and up to 600 °C (**Figure 4** and **Table 2**).

In the TGA curves of all cationic interlayers, the three main weight losses can be ascribed to the elimination of phosphonium group (up to 200 °C), to the aliphatic side chain scission (280–310 °C) and to the macromolecular backbone combustion (up to 370 °C), respectively. In the case of PT6N(EtOH)₂, the first loss of weight (≈10%) is ascribable to diethanolamine group in pendant chain. For interlayer polymers, the percentage of the first weight loss varies from 20% to 40% and this behavior is ascribable to the presence of one or more oxygen atoms linked to the repeating units of the polymeric backbone. CPE polymers, however, can be considered stable enough to be used as photoactive materials in organic photovoltaic devices since the temperature at which they begin to degrade (207 °C in the worst case) are higher than the application temperature.

Thermal properties of polymers have been evaluated by DSC analyses which were carried out under nitrogen atmosphere with a heating ramp of 10 °C min⁻¹ from –20 up to 200 °C (**Table 2**; **Figure S15**, Supporting Information).

All the examined samples show an endothermic flexure, ascribable to the glass transition temperature (T_g). The absence of melting and crystallization phenomena is due to the amorphous nature of the polymers: the tributylphosphonium group linked to the side chains decreases the conformational



Scheme 1. Synthetic routes to obtain the CPE interlayers (PT6buP⁺Br⁻, PTO6buP⁺Br⁻, and P(EDOT-MeO6buP⁺Br⁻)).

Table 1. Polymer characteristics.

Sample	Reaction yield [%]	Postfunctionalization yield ^{a)} [%]	M_n [kDa]	\mathcal{D}
PT6Br	56	–	9.8 ^{b)}	1.9 ^{b)}
PT6buP ⁺ Br ⁻	97	100	17.9 ^{c)}	1.9 ^{c)}
PTO6Br	45	–	2.3 ^{b)}	1.8 ^{b)}
PTO6buP ⁺ Br ⁻	93	100	4.1 ^{c)}	1.8 ^{c)}
P(EDOT-MeO6Br)	31	–	4.3 ^{b)}	1.7 ^{b)}
P(EDOT-MeO6buP ⁺ Br ⁻)	88	100	6.9 ^{c)}	1.7 ^{c)}

^{a)} Determined by ¹H-NMR ^{b)} Determined by GPC chromatography relative to polystyrene standards ^{c)} Calculated from the molecular mass of the corresponding precursors.

order of the polymeric chains with a consequent loss of crystallinity.

Moreover, the possibility to form inter- or intrachain hydrogen bonds when the hydroxylamine substituent is employed increases the T_g value of PT6N(EtOH)₂ sample, even if any clear endothermic melting peak cannot be found.

3.4. Optical Properties

In order to evaluate the optical properties, interlayers and photoactive material were analyzed by UV–vis spectroscopy in solid state (film on quartz slides) and in solution of different polar

solvents (i.e., alcohols and water). The normalized absorption spectra obtained in methanol are reported in **Figure 5** and the maximum absorption wavelengths are reported in **Table 3**. UV–vis analysis was also conducted using other polar solvents (i.e., ethanol and water), and the relative spectra and data are reported in Supporting Information (Figures S16 and S17 and Tables S5 and S6, Supporting Information).

The optical behavior of PT6N(EtOH)₂ is different in solution and in film, due to the change in the conformational order of polymeric chains. In this case, the maximum absorption wavelength shifts from 459 nm (solution) up to 551 nm (film), suggesting that this polymer can achieve highly planar conformations with a high electronic delocalization when in the solid state. Enhanced planarizing interactions can also be ascribed to inter- and intrachain hydrogen bonds, thus leading to an extended conjugation length for this polymer. This behavior is a crucial requirement in view of the final application as electron-donor material in the photoactive layer of polymeric solar cells. On the contrary, the comparison of UV–vis spectra of cationic polymers (CPEs) in solution and in solid state shows only modest shifts of maximum absorption wavelengths.

The UV–vis spectral profiles of cationic polymers are also most independent from the solvent employed for their dissolution and subsequent deposition. In view of this, ethanol was used as the filming solvent for the preparation of cell interlayers due to its low toxicity and with the aim of obtaining more sustainable and eco-friendly devices. Furthermore, an interesting behavior can be observed for P(EDOT-MeO6buP⁺Br⁻) sample, which

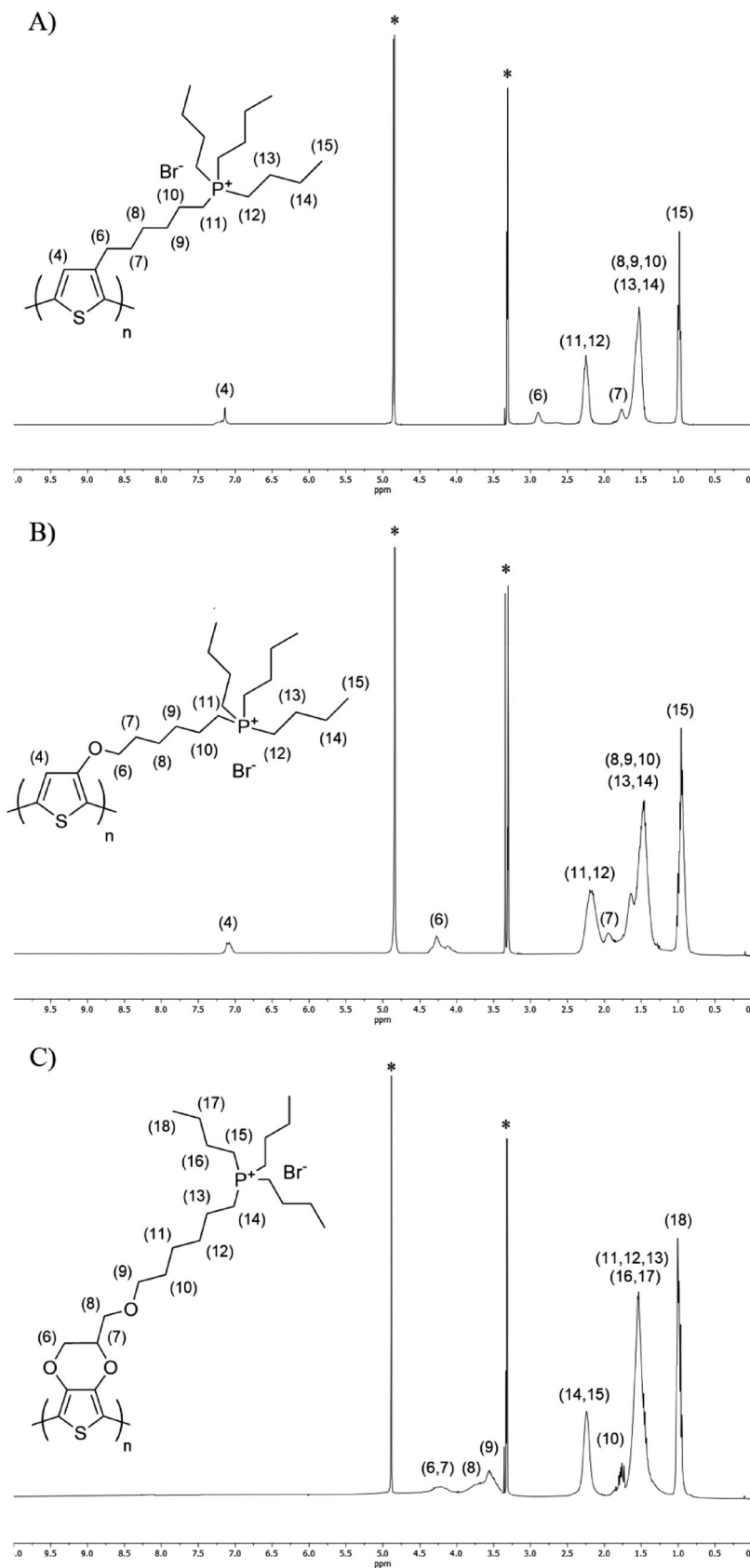


Figure 2. $^1\text{H-NMR}$ spectra of A) $\text{PT6buP}^+\text{Br}^-$, B) $\text{PTO6buP}^+\text{Br}^-$, and C) $\text{P(EDOT-MeO6buP}^+\text{Br}^-)$. Asterisk: solvent resonance (CD_3OD).

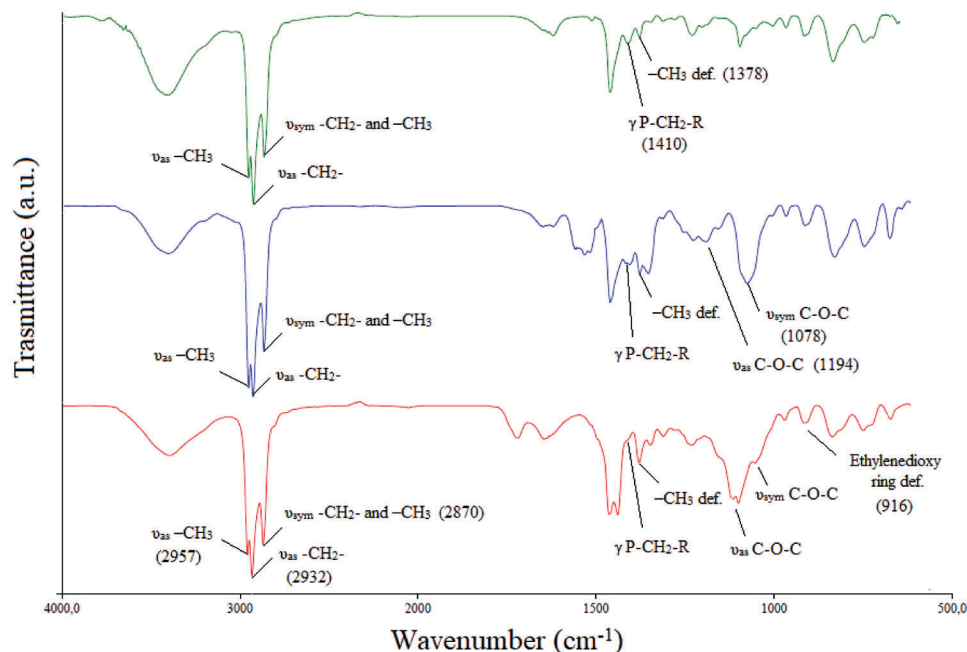


Figure 3. FT-IR spectra of PT6buP⁺Br⁻ (green line), PTO6buP⁺Br⁻ (blue line), and P(EDOT-MeO6buP⁺Br⁻) (red line).

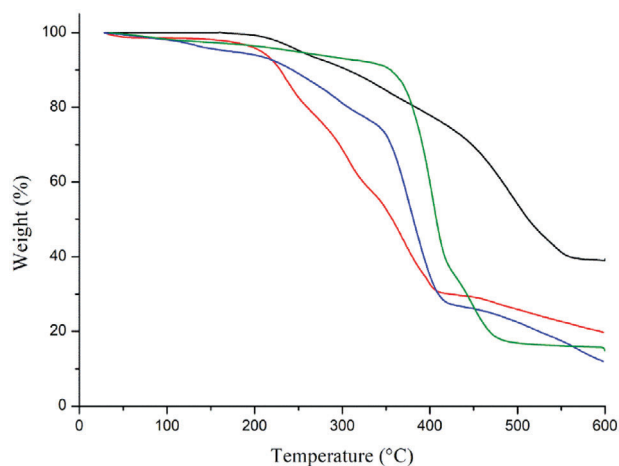


Figure 4. Thermograms of PT6N(EtOH)₂ (black line), PT6buP⁺Br⁻ (green line), PTO6buP⁺Br⁻ (blue line), and P(EDOT-MeO6buP⁺Br⁻) (red line).

Table 2. Decomposition (T_d) and glass-transition (T_g) temperatures of polymers.

Sample	T_d^a [°C]	$T_{d,max}^b$ [°C]	T_g^c [°C]
PT6N(EtOH) ₂	216	253	70
PT6buP ⁺ Br ⁻	373	402	55
PTO6buP ⁺ Br ⁻	217	250	35
P(EDOT-MeO6buP ⁺ Br ⁻)	207	237	32

^{a)} Determined by the onset point of the first inflection ^{b)} Calculated from the first derivative of the weight/temperature curve ^{c)} Evaluated by DSC analysis.

shows structured profiles with three absorption maxima both in solution and in film, suggesting the coexistence of three main chromophores at different conjugation lengths.

3.5. Electrochemical Properties

The potentials of ionic interlayers and neutral photoactive layers (E_{ox}) were evaluated by cyclic voltammetry. Table 4 reports the electrochemical parameters of synthesized polymers in thin films obtained by drop-casting their solution in methanol on Pt electrodes.

The electrochemical properties of the four polymers are quite similar, as they all show irreversible oxidation waves (Figure S18, Supporting Information). However, PTO6buP⁺Br⁻ and P(EDOT-MeO6buP⁺Br⁻) present a lower oxidation potential when compared to the other two polymers. In particular, PTO6buP⁺Br⁻ shows the lowest oxidation potential (+0.47 V) and this can be ascribed to the conjugative effect of the oxygen atom bounded to the thiophenic ring, while the more positive potential (+0.50 V) shown by P(EDOT-MeO6buP⁺Br⁻) is probably due to a balance of inductive and conjugative effects of the two oxygen atoms directly linked to the thiophenic ring.

While the energy levels of the highest occupied molecular orbital (HOMO) of the four polymers were evaluated by CV according to the following equation

$$\text{HOMO (eV)} = -e (E_{ox} + 4.24) \quad (1)$$

where 4.24 V is the saturated calomel electrode (SCE) absolute potential, the energy levels of the lowest unoccupied molecular orbital (LUMO) were evaluated indirectly since the reduction potentials of the four polymers were outside the electrochemical stability window of the electrolyte. LUMO levels were then cal-

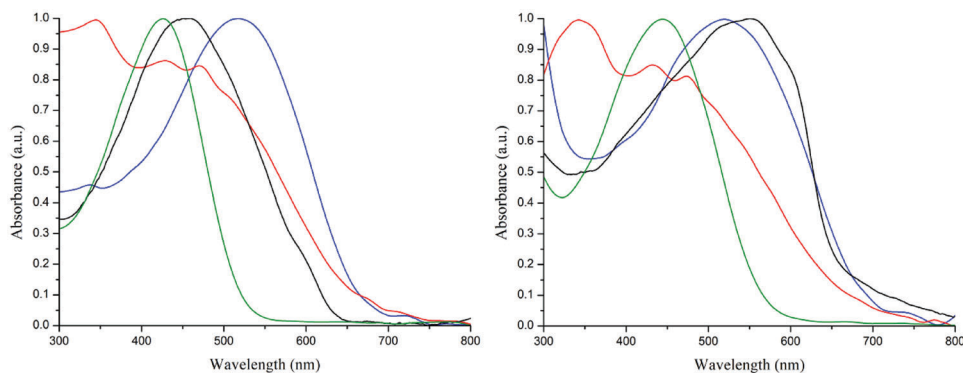


Figure 5. Normalized UV-vis spectra of polymers in methanol solution (left) and in film (right) from MeOH: PT6N(EtOH)₂ (black line), PT6buP⁺Br⁻ (green line), PTO6buP⁺Br⁻ (blue line), and P(EDOT-MeO6buP⁺Br⁻) (red line).

Table 3. Maximum absorption wavelengths (λ_{\max}) of CPEs in solution and thin film.

Sample		λ_{\max} [nm]	
		Solution (10 ⁻⁵ M)	Solid state (film)
PT6buP ⁺ Br ⁻	Methanol	425	445
	Ethanol	426	444
PTO6buP ⁺ Br ⁻	Methanol	518	518
	Ethanol	518	514
P(EDOT-MeO6buP ⁺ Br ⁻)	Methanol	344, 428, 470	342, 432, 473
	Ethanol	348, 426, 469	337, 429, 471

Table 4. Electrochemical and optical properties of synthesized polymers in thin film.

Sample	E_{ox}^{a} [V]	HOMO [eV]	$E_{\text{g, opt}}^{\text{b}}$ [eV]	LUMO [eV]
PT6N(EtOH) ₂	+0.57	-4.81	1.88	-2.93
PT6buP ⁺ Br ⁻	+0.56	-4.80	2.19	-2.61
PTO6buP ⁺ Br ⁻	+0.47	-4.71	1.80	-2.91
P(EDOT-MeO6buP ⁺ Br ⁻)	+0.50	-4.74	1.84	-2.90

^a) Onset potential of anodic scan ^b) Optical bandgap in film.

culated from HOMO levels and the optical bandgaps ($E_{\text{g, opt}}$) obtained from the UV-vis spectra of the films with the equation:

$$\text{LUMO (eV)} = \text{HOMO} + E_{\text{g, opt}} \quad (2)$$

The photoactive polymer and cationic interlayers energy levels and bandgaps suggest comparable degrees of electronic delocalization over the polyconjugated backbones.

3.6. XRD

XRD patterns of polymer films cast on glass slides are shown in **Figure 6**.

All the examined samples show a diffractogram pattern ascribable to an essentially amorphous polymer, according to the absence of evident melting/crystallization peaks evidenced in the thermal analysis section. They only provide for a weak diffrac-

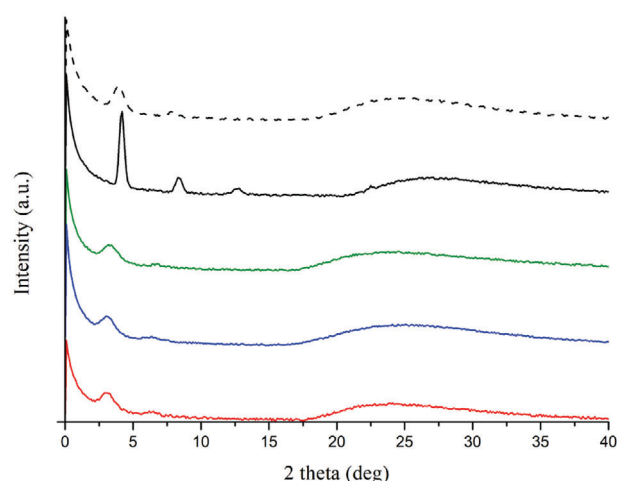


Figure 6. X-ray diffractograms of PT6N(EtOH)₂ not annealed (dashed line) and annealed (black line), PT6buP⁺Br⁻ (green line), PTO6buP⁺Br⁻ (blue line), and P(EDOT-MeO6buP⁺Br⁻) (red line).

tion peak in the 2θ range from 3.11° to 3.93° (**Table 5**), a second one from 6.29° to 7.95°, and a broad amorphous halo at wider angles.

Moreover, their morphological behavior is not affected by the annealing procedure used during the preparation of the photovoltaic cell (heating at 120 °C for 30 min under vacuum). Only sample PT6N(EtOH)₂ not annealed shows an evident increase in crystallinity after annealing (sample PT6N(EtOH)₂ annealed). Indeed, the XRD diffractogram of the latter shows first, second, and third-order reflections at $2\theta = 4.17^\circ$, 8.37° , and 12.6° , corresponding to an intermolecular spacing of polymeric chains on the XY-plane of 21.2 Å (interchain distance) as can be seen in **Table 5**. The small peak at $2\theta = 22.5^\circ$ (3.95 Å) can be ascribed to the π - π stacking distance of PT6N(EtOH)₂ lamellae (**Figure 6**, black line). The photoactive layer can conformationally rearrange its structure towards a more compact and crystalline structure and the achieved more ordered chain conformations can be maintained at room temperature, thanks to the hydrogen bonds between hydroxy groups in the side chains. This hypothesis is also supported by the fact that, after annealing, PT6N(EtOH)₂ films become insoluble in alcohol/water solvents.

Table 5. Structural parameters of polymers.

Sample	Low-angle diffractions [degrees]	High-angle diffractions [degrees]	On plane Th chains distances [Å]	Planes stacking distances [Å]
PT6N(EtOH) ₂ not annealed	3.93; 7.95	–	22.4	–
PT6N(EtOH) ₂ annealed	4.17; 8.37; 12.6	22.5	21.2	3.95
PT6buP ⁺ Br ⁻	3.31; 6.72	–	26.6	–
PTO6buP ⁺ Br ⁻	3.13; 6.33	–	28.2	–
P(EDOT-MeO6buP ⁺ Br ⁻)	3.11; 6.29	–	28.4	–

Table 6. Short-circuit current density (J_{sc}), open-circuit voltage (V_{oc}), fill factor (FF), power conversion efficiency (PCE), parallel resistance (R_p), and series resistance (R_s) of tested photovoltaic devices. Average performances are taken from ten devices.

Sample	J_{sc} [mA cm ⁻²]	V_{oc} [V]	FF	PCE [%]	R_p [Ohm cm ⁻²]	R_s [Ohm cm ⁻²]
PT6N(EtOH) ₂	9.77 ± 0.14	0.58 ± 0.01	0.57 ± 0.02	3.23 ± 0.22	170 ± 18	5.5 ± 0.22
PT6N(EtOH) ₂ /PT6buP ⁺ Br ⁻	12.1 ± 0.15	0.60 ± 0.01	0.58 ± 0.03	4.21 ± 0.18	260 ± 22	2.2 ± 0.16
PT6N(EtOH) ₂ /P(EDOT-MeO6buP ⁺ Br ⁻)	12.6 ± 0.18	0.61 ± 0.01	0.59 ± 0.01	4.54 ± 0.19	280 ± 21	1.5 ± 0.11
PT6N(EtOH) ₂ /PTO6buP ⁺ Br ⁻	13.2 ± 0.16	0.62 ± 0.01	0.61 ± 0.03	4.99 ± 0.16	490 ± 21	0.8 ± 0.09

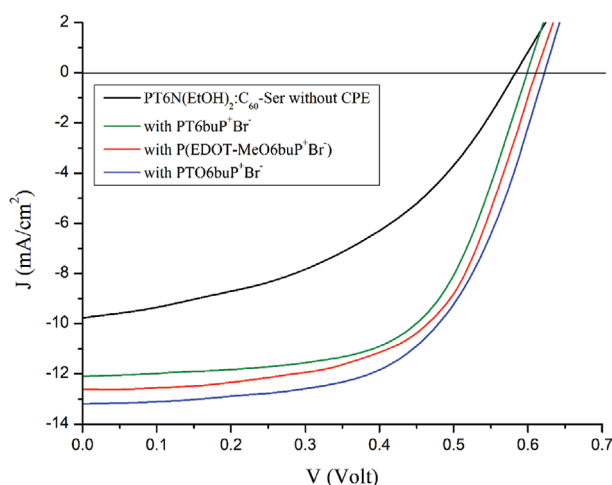


Figure 7. Current density–voltage (J/V) for the best-performing cells tested under AM 1.5 one-sun illumination.

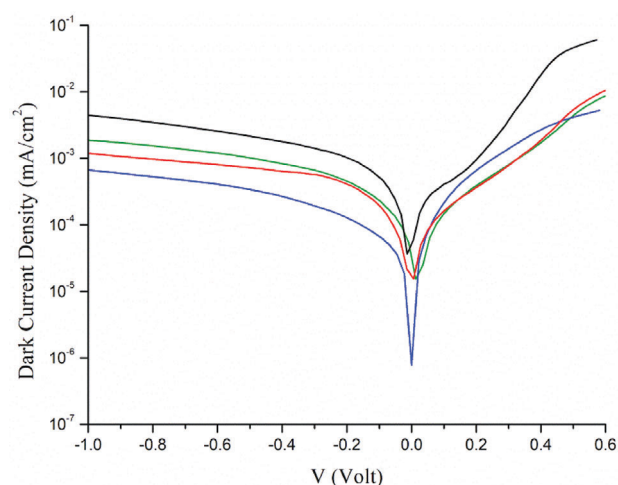


Figure 8. Semilogarithmic current density versus voltage curves of the prepared devices measured in the dark: PT6N(EtOH)₂ (black line), PT6buP⁺Br⁻ (green line), PTO6buP⁺Br⁻ (blue line), and P(EDOT-MeO6buP⁺Br⁻) (red line).

3.7. Photovoltaic Properties

Cationic alcohol-soluble polymers (PT6buP⁺Br⁻, PTO6buP⁺Br⁻, and P(EDOT-MeO6buP⁺Br⁻)) were tested as electron transport interlayers for the obtainment of green BHJ solar cells based on a photoactive layer composed by PT6N(EtOH)₂ and C₆₀-Ser. Photovoltaic properties were investigated by adopting the device configuration ITO/PEDOT:PSS/photoactive layer/CPE/Al. PT6N(EtOH)₂ was used in a 1:1 weight ratio blend with C₆₀-Ser, while CPEs were filmed from an ethanol solution (2.0 mg mL⁻¹). The increased crystallinity of PT6N(EtOH)₂ after the annealing procedure allowed to avoid the protection of the photoactive layer during the interlayer deposition. Photovoltaic performance parameters are shown in Table 6, while J/V curves are reported in Figure 7.

Taking as a reference the photovoltaic device composed by photoactive blend (PT6N(EtOH)₂:C₆₀-Ser) and devoid of any cationic interlayer, from Table 6 and Figure 6, it is evident that the photovoltaic parameters obtained from cells prepared with CPE interlayers notably increase, and this is particularly true for the current density. The effect of CPE interlayers on the interface between the cell active layer and the Al cathode can be ascribed to the interactions between PT6N(EtOH)₂ and the cationic polymer, which enhances the electron injection to the Al cathode.^[37] Moreover, the enhancement of V_{oc} can be ascribed to the reduction in the electrode (Al) work function owing to the formation of an interfacial dipole between the cathode interlayer and the metal, induced by the presence of ionic salts in the side chains of the employed cationic polythiophenes. Indeed, at cathodes with an

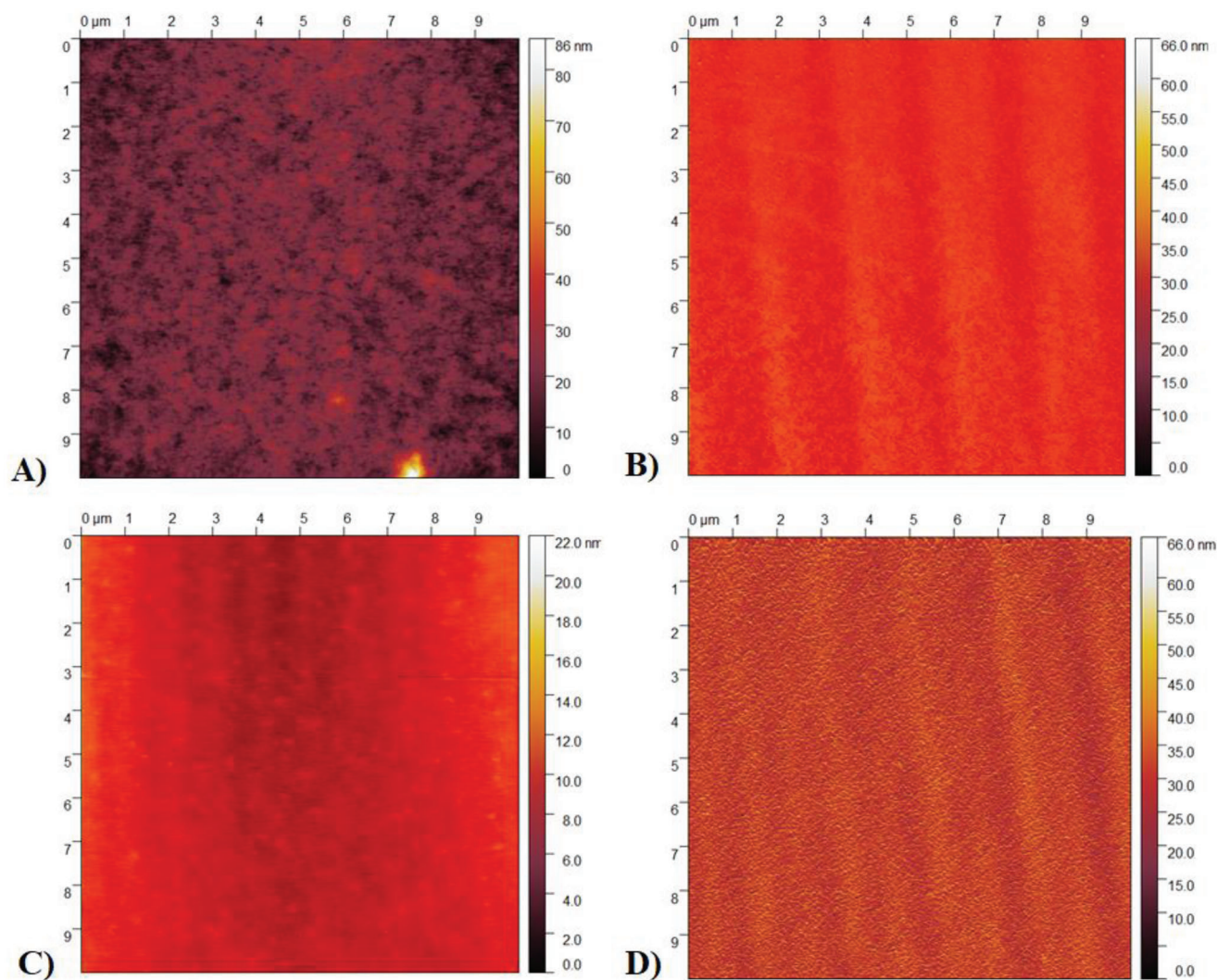


Figure 9. AFM topography images of A) PT6N(EtOH)₂ layer and of PT6N(EtOH)₂ after spray-coating of B) PT6buP⁺Br⁻, C) PTO6buP⁺Br⁻, and D) P(EDOT-MeO6buP⁺Br⁻) outer layer.

interfacial layer composed of a tetraalkylphosphonium bromide polythiophene derivative, the ohmic contact with the electrons transported from the photoactive layer to the metal electrode is enhanced.^[38]

Best results were obtained using the PTO6buP⁺Br⁻ interlayer with an improvement of PCE of 55% with respect to the reference device. These results are particularly promising since all prepared polymers can be easily synthesized, their deposition does not require the use of toxic or harmful solvents (chlorinates and aromatics), and the simple solution process can be a wide practicable methodology for the development of efficient and sustainable OPV solar cells.

The electrical behavior of the prepared cells has also been examined in the dark, and the resulting curves are reported in **Fig. 8**.

The leakage current difference between the device without interlayer and those with the cationic interlayer is about one order of magnitude. The reduced dark current after the insertion

of the interlayer can be attributed to the charge-blocking properties of the employed cationic-polythiophene materials, which can induce a positive shift of the cell built-in voltage (Table 6).^[39] Moreover, the low dark current densities observed with the hole blocking layers indicate that the bimolecular recombination is reduced, thus leading to a higher photocurrent.^[40]

The incorporation of an interlayer in photovoltaic devices can also influence their electrical characteristics and the relevant diode parameters. Series resistance (R_s) and parallel (shunt) resistance (R_p)—summarized in Table 6—were obtained by the inverse gradient of the J/V curve at the short circuit and the open circuit under illumination, respectively. After the incorporation of the cationic interlayers, R_s values decrease while R_p values increase, indicating that the ionic polythiophenes can effectively reduce the bimolecular recombination in organic solar cells.^[41]

Based on the obtained results, the highest device efficiencies have been achieved with PTO6buP⁺Br⁻ interlayer, which is able to positively interact with PT6N(EtOH)₂, leading to a reduced

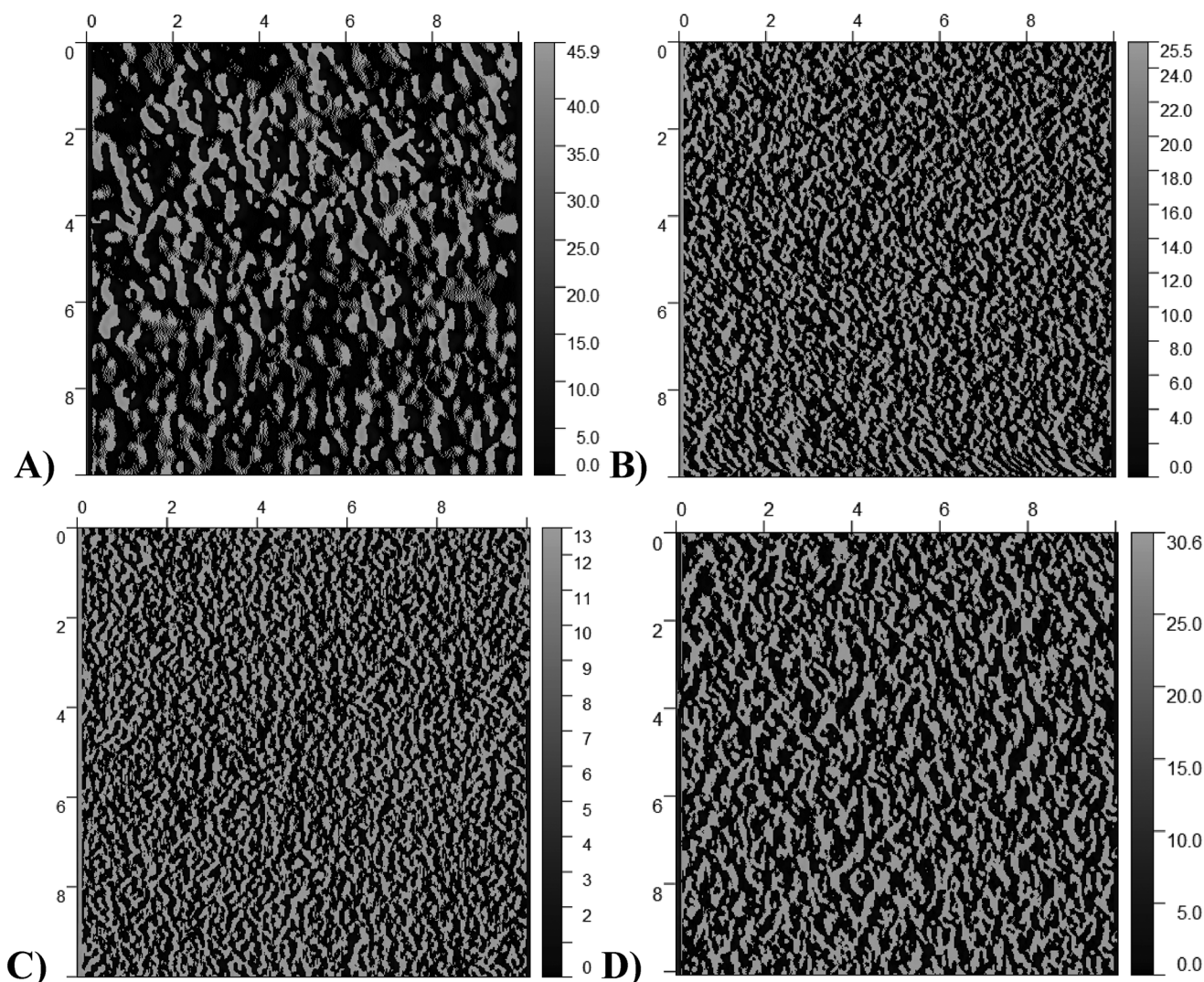


Figure 10. AFM phase images ($10 \times 10 \mu\text{m}$; z-scale: in degrees) of A) PT6N(EtOH)₂ layer and of PT6N(EtOH)₂ after spray-coating of B) PT6buP⁺Br⁻, C) PTO6buP⁺Br⁻, and D) P(EDOT-MeO6buP⁺Br⁻) outer layer.

hole–electron recombination in the photoactive layer as well as an increased electron extraction from C₆₀-Ser to the cathode.

3.8. Morphological Characterization

The morphology of the examined solar cells has been evaluated by the investigation of the surface nano-topography using AFM technique. **Figure 9A** shows the image of the active layer film (PT6N(EtOH)₂) after the annealing procedure. The surface RMS roughness is 10.2 nm, and the observed phase separation can be ascribed to the presence of polymer crystallites, as already evidenced by XRD measurements. The deposition of CPE layers on the active surface decreases the surface roughness leading to RMS values of 7.07, 5.08, and 6.03 nm with PT6buP⁺Br⁻, PTO6buP⁺Br⁻, and P(EDOT-MeO6buP⁺Br⁻), respectively (**Figure 9B–D**). Moreover, the high affinity of the CPE with respect to the underlying active layer leads to the complete coverage of the

photoactive film, an important requisite to achieve high performance of the OPV device.^[42] These results are also confirmed by AFM phase images (**Figure 10**) where PT6N(EtOH)₂ active layer blend film shows a coarse structure with phase-separated and distinct domains (**Figure 10A**), owing both to the nanoscale assembly of PT6N(EtOH)₂ and C₆₀-Ser and the partial crystallization of the ED polymer. After the deposition of cationic interlayers (**Figure 10B–D**), the surface of the obtained films was almost amorphous and featureless, according with what reported for topographic AFM analysis.

3.9. EQE Measurements

Further confirmation of the increment of electron extraction efficiency by the insertion of cathodic layers is given by the analysis of the EQE spectra reported in **Figure 11**. The photovoltaic cell without interfacial layer (red line) shows an EQE in the

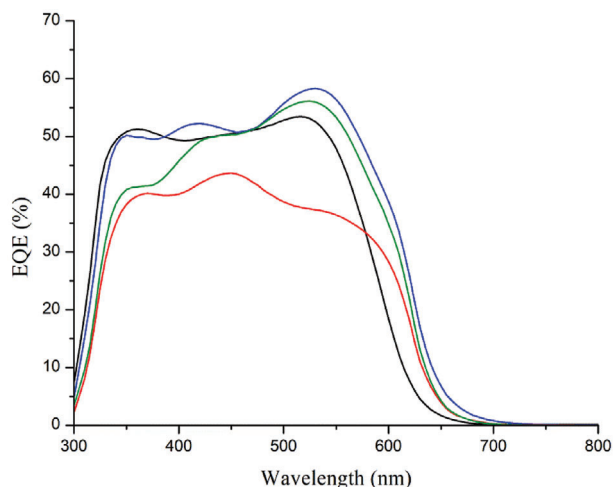


Figure 11. EQE spectra of the tested devices: PT6N(EtOH)₂:C₆₀-Ser without (red line) and with interlayer: PT6buP⁺Br⁻ (green line), PTO6buP⁺Br⁻ (blue line), and P(EDOT-MeO6buP⁺Br⁻) (black line).

350–650 nm range of $\approx 40\%$, while those with CPE reach an EQE of ≈ 52 – 58% . In particular, the cell with PTO6buP⁺Br⁻ as an interfacial layer (blue line) shows a wide absorption (300–660 nm) and the higher value of quantum efficiency. The obtained results are in good agreement with the improvement in photocurrent reported in Table 6 when interlayers are employed.

4. Concluding Remarks

Three polythiophenes functionalized with a tetraalkylphosphonium bromide cationic group—poly[3-(6-tributylphosphoniumhexyl)thiophene]bromide, poly[3-(6-tributylphosphoniumhexyloxy)thiophene]bromide and poly(6-tributylphosphoniumhexyl-1-oxymethyl-EDOT)bromide—were successfully synthesized, through a simple and effective post-polymerization functionalization reaction on the corresponding ω -alkylbrominated polymeric precursors obtained by oxidative polymerization with iron trichloride. The prepared CPEs, well soluble in polar solvents (water/alcohols), were then employed as cathode interlayers in BHJ photovoltaic solar cells based on the photoactive water/alcohol soluble blend made of poly[3-(6-diethanolaminoethyl)thiophene] and the serinol-functionalized fullerene derivative (C₆₀-Ser). The comparison of photovoltaic parameters of the reference device with those of the cells with cathode interlayers showed that the insertion of the CPE improves photoconversion efficiency, and this is particularly true for the cell employing poly[3-(6-tributylphosphoniumhexyloxy)thiophene]bromide as electron-transfer polymer, achieving an efficiency increase of 55%. Electrical measurements revealed an increase in charge collection efficiency and in exciton dissociation rate, while the AFM measurements evidenced that CPEs afforded a complete coverage of the photoactive layers, owing to the high physicochemical affinity between the two polymeric layers.

This work demonstrates that the right choice of the fundamental components of a polymeric solar cell can give promising results not only in terms of photoconversion efficiency but also re-

garding the environmental impact during the assembly of the final device.

Supporting Information

Supporting Information is available from the Wiley Online Library or from the author.

Acknowledgements

This work was funded by the Canaletto programme (Grant No. PPN/BIL/2018/2/00035/U/00001), through the National Agency for Academic Exchange (NAWA), by the Italian Ministry of Foreign Affairs and International Cooperation (Farnesina), Project PO19MO13, by the First TEAM (Grant No. POIR.04.04.00-00-5ED7/18-00), within the framework of the First TEAM program of the Foundation for Polish Science (FNP), cofinanced by the European Union under the European Regional Development Fund. The financial support from the University of Bologna is gratefully acknowledged.

Conflict of Interest

The authors declare no conflict of interest.

Data Availability Statement

The data that support the findings of this study are available in the supplementary material of this article.

Keywords

conjugated polyelectrolyte, electron transport layers, polythiophene, water/alcohol-soluble polymers

Received: November 21, 2022

Revised: January 10, 2023

Published online: January 29, 2023

- [1] H.-L. Yip, A. K.-Y. Jen, *Energy Environ. Sci.* **2012**, *5*, 5994.
- [2] K. A. Mazzio, C. K. Luscombe, *Chem. Soc. Rev.* **2015**, *44*, 78.
- [3] G. Dennler, M. C. Scharber, C. J. Brabec, *Adv. Mater.* **2009**, *21*, 1323.
- [4] A. Sharma, D. Pathak, D. P. Sharma, J. M. Nunzi, *Eur. Phys. J.: Appl. Phys.* **2022**, *97*, 81.
- [5] X. Zhang, H. Zhang, Y. Li, S.-U. Zafar, S. Yang, J. Chen, H. Zhou, Y. Zhang, *Adv. Funct. Mater.* **2022**, *32*, 2205398.
- [6] F. Zhang, M. Johansson, M. R. Andersson, J. C. Hummelen, O. Inganäs, *Adv. Mater.* **2002**, *14*, 662.
- [7] K. Suemori, T. Miyata, M. Yokoyama, M. Hiramoto, *Appl. Phys. Lett.* **2004**, *85*, 6269.
- [8] J. H. Seo, A. Gutacker, Y. Sun, H. Wu, F. Huang, Y. Cao, U. Scherf, A. J. Heeger, G. C. Bazan, *J. Am. Chem. Soc.* **2011**, *133*, 8416.
- [9] Y. Zhao, Z. Xie, C. Qin, Y. Qu, Y. Geng, L. Wang, *Sol. Energy Mater. Sol. Cells* **2009**, *93*, 604.
- [10] J. Luo, H. B. Wu, C. He, A. Y. Li, W. Yang, Y. Cao, *Appl. Phys. Lett.* **2009**, *95*, 043301.
- [11] H. Zeng, X. Zhu, Y. Liang, X. Guo, *Polymers* **2015**, *7*, 333.
- [12] H. Wu, F. Huang, Y. Mo, W. Yang, D. Wang, J. Peng, Y. Cao, *Adv. Mater.* **2004**, *16*, 1826.

- [13] J. Kesters, S. Govaerts, G. Pirotte, J. Drijkoningen, M. Chevrier, N. Van Den Brande, X. Liu, M. Fahlman, B. Van Mele, L. Lutsen, D. Vanderzande, J. Manca, S. Clément, E. Von Hauff, W. Maes, *ACS Appl. Mater. Interfaces* **2016**, *8*, 6309.
- [14] B. H. Lee, I. H. Jung, H. Y. Woo, H.-K. Shim, G. Kim, K. Lee, *Adv. Funct. Mater.* **2014**, *24*, 1100.
- [15] Y. Wu, Y. Liu, T. Emrick, T. P. Russell, *Prog. Polym. Sci.* **2020**, *103*, 101222.
- [16] Z. He, C. Zhong, X. Huang, W.-Y. Wong, H. Wu, L. Chen, S. Su, Y. Cao, *Adv. Mater.* **2011**, *23*, 4636.
- [17] M. Lanzi, E. Salatelli, L. Giorgini, A. Mucci, F. Pierini, F. P. Di-Nicola, *Eur. Polym. J.* **2017**, *97*, 378.
- [18] M. Lanzi, E. Salatelli, L. Giorgini, M. Marinelli, F. Pierini, *Polymer* **2018**, *149*, 273.
- [19] M. Fossépré, M. E. Trévisan, V. Cyriaque, R. Wattiez, D. Beljonne, S. Richeter, S. Clément, M. Surin, *ACS Appl. Bio Mater.* **2019**, *2*, 2125.
- [20] H. A. Ho, M. Leclerc, *J. Am. Chem. Soc.* **2003**, *125*, 4412.
- [21] S.-H. Oh, S.-I. Na, Y.-C. Nah, D. Vak, S.-S. Kim, D.-Y. Kim, *Org. Electron.* **2007**, *8*, 773.
- [22] C. Duan, K. Zhang, C. Zhong, F. Huang, Y. Cao, *Chem. Soc. Rev.* **2013**, *42*, 9071.
- [23] C. Costa, J. Farinhas, M. F. G. Velho, J. Avó, M. Matos, A. M. Galvão, A. Charas, *New J. Chem.* **2019**, *43*, 14246.
- [24] J. Chang, S.-J. Zhang, Y.-W. Jiang, L. Xu, J.-M. Yu, W.-J. Zhou, X. Sun, *ChemMedChem* **2013**, *8*, 976.
- [25] R. S. Loewe, P. C. Ewbank, J. Liu, L. Zhai, R. D. McCullough, *Macromolecules* **2001**, *34*, 4324.
- [26] M. Lanzi, E. Salatelli, M. Marinelli, F. Pierini, *Macromol. Chem. Phys.* **2020**, *221*, 1900433.
- [27] C. Xie, L. Chen, Y. Chen, *J. Phys. Chem. C* **2013**, *117*, 24804.
- [28] G. Marzano, F. Carulli, F. Babudri, A. Pellegrino, R. Po, S. Luzzati, G. M. Farinola, *J. Mater. Chem.* **2016**, *4*, 17163.
- [29] C.-J. Lee, H. Wang, M. Young, S. Li, F. Cheng, H. Cong, G. Cheng, *Acta Biomater.* **2018**, *75*, 161.
- [30] M. Lanzi, D. Quadretti, M. Marinelli, Y. Ziai, E. Salatelli, F. Pierini, *Polymers* **2021**, *13*, 1640.
- [31] M. Marinelli, M. Lanzi, F. Pierini, Y. Ziai, A. Zanelli, D. Quadretti, F. Di Maria, E. Salatelli, *Polymers* **2022**, *14*, 3965.
- [32] C. Xie, L. Chen, Y. Chen, *J. Phys. Chem. C* **2013**, *117*, 24804.
- [33] J. Roncali, *Chem. Rev.* **1992**, *92*, 711.
- [34] S. Hladys, A. Murmiliuk, J. Vohlídal, D. Havlíček, V. Sedlářík, M. Štěpánek, J. Zedník, *Eur. Polym. J.* **2018**, *100*, 200.
- [35] S. Hladys, D. Bondarev, J. Svoboda, J. Vohlídal, D. Vrbata, J. Zedník, *Eur. Polym. J.* **2016**, *83*, 367.
- [36] S. Bishnoi, R. Datt, S. Arya, S. Gupta, R. Gupta, W. C. Tsoi, S. N. Sharma, S. P. Patole, V. Gupta, *Adv. Mater. Interfaces* **2022**, *9*, 2101693.
- [37] L. Zhang, C. He, J. Chen, P. Yuan, L. Huang, C. Zhang, W. Cai, Z. Liu, Y. Cao, *Macromolecules* **2010**, *43*, 9771.
- [38] S.-I. Na, S.-H. Oh, S.-S. Kim, D.-Y. Kim, *Org. Electron.* **2009**, *10*, 496.
- [39] J. Luo, H. B. Wu, C. He, A. Y. Li, W. Yang, Y. Cao, *Appl. Phys. Lett.* **2009**, *95*, 043301.
- [40] X. Gong, M. Tong, F. G. Brunetti, J. Seo, Y. Sun, D. Moses, F. Wudl, A. J. Heeger, *Adv. Mater.* **2011**, *23*, 2272.
- [41] C. J. Brabec, V. Dyakonov, J. Parisi, N. S. Sariciftci, in *Organic Photovoltaics, Concepts and Realization*, Vol. 10, Springer, New York **2003**, pp. 151–153.
- [42] J. Kesters, S. Govaerts, G. Pirotte, J. Drijkoningen, M. Chevrier, N. Van Den Brande, X. Liu, M. Fahlman, B. Van Mele, L. Lutsen, D. Vanderzande, J. Manca, S. Clément, E. Von Hauff, W. Maes, *ACS Appl. Mater. Interfaces* **2016**, *8*, 6309.